https://doi.org/10.5194/egusphere-2022-1243
Preprint. Discussion started: 22 November 2022

Breakups are Complicated: An Efficient Representation of Collisional Breakup in the Superdroplet Method

Emily de Jong[1], J. Ben Mackay[2,3], Anna Jaruga[2], and Sylwester Arabas[4]

[1]Department of Mechanical and Civil Engineering, California Institute of Technology, Pasadena, CA, USA
[2]Department of Environmental Science and Engineering, California Institute of Technology, Pasadena, CA, USA
[3]Scripps Institution of Oceanography, San Diego, CA, USA
[4]Faculty of Mathematics and Computer Science, Jagiellonian University, Kraków, Poland

Correspondence: Emily de Jong (edejong@caltech.edu)

Abstract. A key constraint of particle-based methods for modeling cloud microphysics is the conservation of total particle number, which is required for computational tractability. The process of collisional breakup poses a particular challenge to this framework, as breakup events often produce many droplet fragments of varying sizes, which would require creating new particles in the system. This work introduces a representation of collisional breakup in the so-called "superdroplet" method which conserves the total number of superdroplets in the system. This representation extends an existing stochastic collisional-coalescence scheme and samples from a fragment-size distribution in an additional Monte Carlo step. This method is demonstrated in a set of idealized box model and single-column warm-rain simulations. We further discuss the effects of the breakup dynamic and fragment-size distribution on the particle size distribution, hydrometeor population, and microphysical process rates. This representation of collisional breakup is able to produce a stationary particle-size distribution, in which breakup and coalescence rates are approximately equal, and it recovers expected behavior such as precipitation suppression in the column model. Furthermore, representing breakup has potential benefits that extend beyond warm rain processes, such as the ability to capture mechanisms of secondary ice production in the superdroplet method. The breakup algorithm presented here contributes to an open-source pythonic implementation of the superdroplet method, 'PySDM', which will facilitate future research using particle-based microphysics.

1 Introduction

The superdroplet method (SDM) for cloud microphysics is a high-fidelity particle-based (Lagrangian) representation of aerosols and hydrometeors that offers notable advantages over traditional bulk and bin microphysics schemes. Particle-based methods were initially used in atmospheric simulations to represent ice nucleation (Paoli et al., 2004; Jensen and Pfister, 2004; Shirgaonkar and Lele, 2006; Sölch and Kärcher, 2010), and were later extended to study aerosol indirect effects with a superdroplet approach (Andrejczuk et al., 2008) in which each "superdroplet" represents a mutliplicity of modeled particles with identical attributes, such as size and chemical properties. Later, the SDM was extended to include a stochastic representation of collisional coalescence (Shima et al., 2009; Riechelmann et al., 2012) and ice-phase processes (Shima et al., 2020), making the SDM a nearly-complete Monte Carlo representation of cloud microphysics. The burgeoning field of particle-based cloud microphysics

https://doi.org/10.5194/egusphere-2022-1243
Preprint. Discussion started: 22 November 2022

uses SDM implementations in large-eddy simulations (LES) to understand microphysical processes that are underresolved in traditional bulk and bin methods (e.g., Chandrakar et al., 2021; Andrejczuk et al., 2010; Morrison et al., 2019; Dziekan et al., 2019; Grabowski, 2020; Hoffmann, 2017). Furthermore, a growing literature of machine learning in microphysics utilizes the SDM as a source of high-fidelity training data from which to "learn" microphysical tendencies and properties (Bieli et al., 2022; Seifert and Rasp, 2020). However, without a complete representation of microphysical processes in the SDM, its predictive and benchmarking power for cloud feedbacks is limited.

Many implementations of the SDM do not include the process of collisional breakup of droplets. Not only is collisional breakup a highly uncertain process in existing bin and bulk parameterizations (Morrison et al., 2020; Grabowski et al., 2019), but these uncertainties have been found to impact rain rates and other macroscale quantities in bin microphysics studies (Seifert et al., 2005). Studying collisional breakup in the SDM is not straightforward – a single breakup event is likely to produce fragments of multiple different sizes. A naive representation of all fragments in the SDM would require the creation of new superdroplet tracers in the system, which can lead to an explosive growth of superdroplet quantity and dramatically inhibit performance of the SDM. Scalability of the SDM for parallel applications such as LES requires a conservation of the total number of superdroplets. This work proposes a superdroplet-conserving SDM algorithm for the representation of collisional breakup, using a Monte Carlo step that samples from a fragment size distribution.

This superdroplet-conserving breakup implementation draws inspiration from an analogous "superparticle" representation of phytoplankton (Jokulsdottir and Archer, 2016): individual phytoplankton aggregates spontaneously break uniformly into a number of fragments determined by a power law probability distribution. We apply a similar spontaneous breakup principle to an intermediate coalesced state resulting from the collision of two droplets. (While spontaneous breakup of water droplets has also been investigated (Kamra et al., 1991), it has not been observed in in-situ studies of cloud droplet collisions (Testik and Rahman, 2017) and is widely considered insignificant for atmospheric microphysics (Rogers and Yau, 1989).) The presented collisional breakup algorithm utilizes empirical collection/breakup efficiencies (such as Schlottke et al. (2010); Beard and Ochs (1995); Berry (1967)) to determine whether a colliding droplet pair is likely to break-up, and then samples from a corresponding empirical fragment size distribution (such as Low and List (1982); Schlottke et al. (2010); Beard and Ochs (1995); McFarquhar (2004)) to determine the properties of the resulting fragmented superdroplet. Breakup parameterizations are typically very complex and aim to summarize multiple physical mechanisms of breakup. This work addresses how the proposed SDM breakup algorithm samples from such complex fragment size distributions, but leaves evaluation and analysis of these empirical distributions to future work.

The contents of this paper proceed as follows: Section 2 begin with a conceptual description of the proposed breakup algorithm, followed by a mathematical description of its implementation. Section 3 then presents several idealized simulations including various parameterizations of collisional breakup to demonstrate the behavior of this implementation in the SDM. Section 4 concludes the discussion and poses additional scientific questions which may be within reach given this novel implementation.

https://doi.org/10.5194/egusphere-2022-1243
Preprint. Discussion started: 22 November 2022

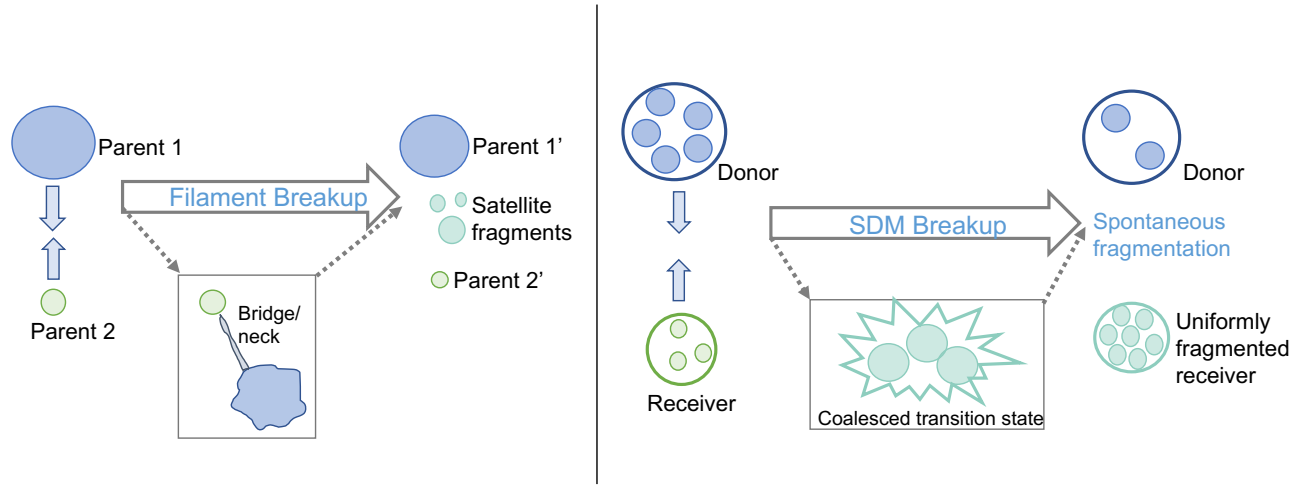

Figure 1. Conceptual view of a real filament breakup event (left) and the tracer-conserving SDM collisional breakup dynamic described in this work (right). The real event involves collision between two individual droplets, which may form a neck bridging each other before fragmenting into several differently sized droplets, consisting of derivatives of the initial colliding parents, plus a set of small fragments known as "satellites." The tracer-conserving SDM representation involves collision of two groups of droplets (each group represented as one superdroplet, a donor and receiver), which collide and coalescence into a transition state, which then fragments uniformly. The result of the SDM breakup is two superdroplets, or two groups of droplets, with one group corresponding to leftover donor droplets, and the other group corresponding to a set of fragments whose size has been sampled from the overall fragment size distribution.

2 Superdroplet-conserving Collisional Breakup

2.1 Conceptual description

Two colliding liquid hydrometeors in the atmosphere can break-up via several physical pathways, including filament, sheet, and disc breakup (Barros et al., 2008). The colliding droplets, referred to as "parents", typically lose mass to newly-formed tiny "satellite" droplets that result from the collision, thereby resulting in several differently sized droplet fragments (see figure 1, left). As noted previously, scaling of the SDM relies on preserving the number of tracers in the system. In order to preserve the number of superdroplets in a binary collisional breakup event, breakup is treated as a two step process based on superdroplet-conserving coalescence (figure 1, right). First, the two superdroplets collide and coalesce: the superdroplet of higher multiplicity acts as a "donor“ by donating mass and multiplicity while maintaining its attributes; the other superdroplet acts as a "receiver“ by growing in mass and maintaining its multiplicity to form a "coalesced transition state." This unstable coalesced transition state immediately breaks up into fragments of uniform size: the attributes and multiplicity of this fragmented receiver are updated, with multiplicity increasing and mass of the individual droplets represented by the superdroplet decreasing. Uniform fragmentation is required to maintain conservation of superdroplets. Furthermore, uniform fragmentation requires the assumption that all superparticle attributes are extensive quantities and undergo equipartitional splitting (not ap-

https://doi.org/10.5194/egusphere-2022-1243
Preprint. Discussion started: 22 November 2022

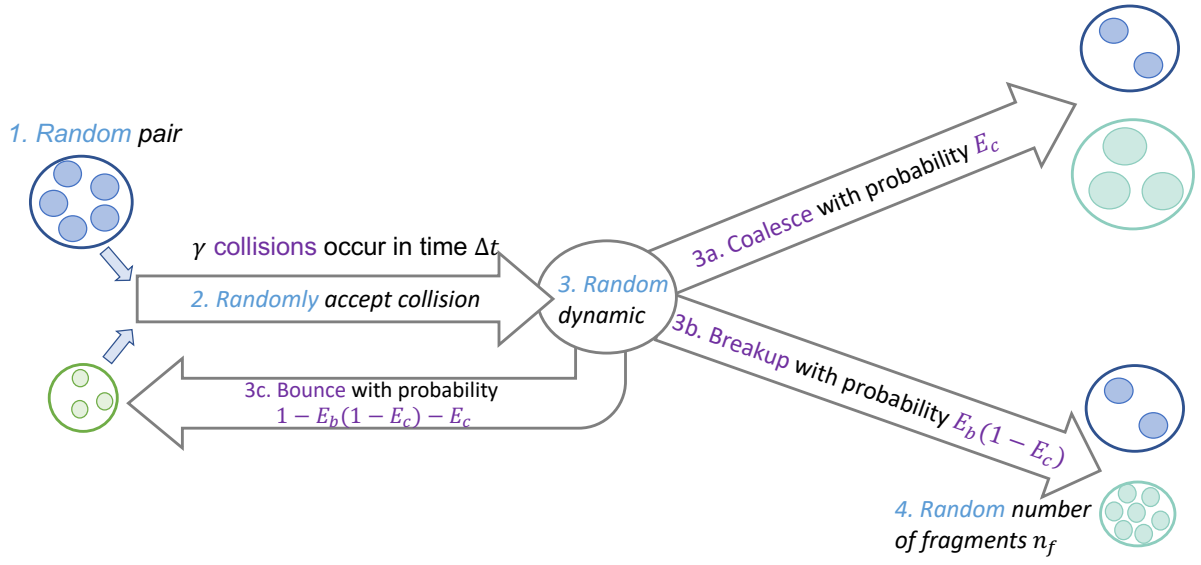

Figure 2. Diagram of the Monte Carlo decision pathway during a collision-coalescence-breakup event in the proposed algorithm.

plicable, e.g., for insoluble aerosol constituents). The product of a collisional breakup event is therefore two superdroplets: the donor maintains its attributes but donates multiplicity, and the fragmented receiver represents (uniform) fragments that result from the breakup event following a coalesced transition state. As in the original Monte Carlo step that determines whether a collision occurs, the fragment size is sampled at random from a fragment size distribution, which may depend on the properties of the colliding particles.

2.2 Mathematical description

The superdroplet-conserving method of collisional breakup is illustrated in figure 2 and formulated below using notation following work of Shima et al.. A single superdroplet with label i has a position $\mathbf{x}_i(t)$ and extensive physical attributes $\mathbf{a}_i(t)$, such as volume or mass ($V_i(t), M_i(t)$, respectively). Each superdroplet corresponds to a multiplicity $\xi_i(t)$ of "real" droplets which exist in the same gridbox and have identical such attributes.

The proposed breakup algorithm unifies the representation of collisional coalescence and breakup and builds on the original coalescence Monte Carlo steps in Shima et al.. As in this original SDM, we begin by selecting pairs of superdroplets to consider collisions:

1. All superdroplets within a cell are randomly ordered in a list of non-overlapping pairs (j_α, k_α) where j and k are the superdroplet indices, and α refers to the pair index.

Next, we determine how many collisions, γ_α, occur for the pair α in the time step:

https://doi.org/10.5194/egusphere-2022-1243
Preprint. Discussion started: 22 November 2022

2. The probability of collision between droplets i and j is given by

$$P_{i,j} = K_{i,j}\Delta t \tag{1}$$

where $K_{i,j}$ is the rate of collisions based on the properties of droplets i and j, and Δt is the model time step. The scaled probability of collision $P_\alpha^{(s)}$ for this pair α accounts for the multiplicities of the colliding superdroplets:

$$P_\alpha^{(s)} = \max(\xi_j, \xi_k) P_\alpha. \tag{2}$$

Only a subset $\lfloor n_s/2 \rfloor$ of possible SD pairs are considered out of all possible superdroplet pairs at each time step. Therefore, the probability is further scaled up to form the corrected probability of collision:

$$p_\alpha = \frac{n_s(n_s-1)}{2} / \lfloor \frac{n_s}{2} \rfloor P_\alpha^{(s)}. \tag{3}$$

The number of collisions that occur in this time step, γ_α, is then determined in a Monte Carlo step based on p_α. Taking $\phi_\alpha \in (0,1)$ to be a uniform random number,

$$\gamma_\alpha = \min(\lceil p_\alpha - \phi_\alpha \rceil, \lfloor \xi_{j_\alpha} / \xi_{k_\alpha} \rfloor). \tag{4}$$

Here, we assumed the superdroplets are ordered such that $\xi_{j_\alpha} \geq \xi_{k_\alpha}$. If $\gamma_\alpha = 0$, then no collisions occur.

The collision rate is then γ_α collisions per gridbox and per time step. Due to the constraint in equation (4) based on droplet multiplicity, some collisions which should occur probabilistically cannot if the donor superdroplet has insufficient multiplicity to collide p_α times. Therefore, a collision deficit $p_\alpha - \gamma_\alpha$ may be tracked as a tool to assess whether the model time step is sufficiently small (elimination of the the collision deficit is used for adaptive step size control in the SDM implementation used herein (Arabas et al., 2022)).

In the original SDM, particles coalesce as long as $\gamma_\alpha > 0$, as the rate of collisions is taken to refer only to collisional coalescence. However, when we consider collisional breakup, an additional Monte Carlo step must be taken to determine whether the particles coalesce or break up. This is determined based on a coalescence efficiency (or collection efficiency) E_c, which generally depends on properties of the colliding particles such as their fall speed, mass, and surface tension. We additionally account for the fact that in some collisions, droplets may bounce off of one another elastically by including an optional additional parameter for the breakup efficiency, E_b. This second Monte Carlo step is summarized as follows.

3. Compute the dynamic that occurs: coalescence, breakup, or bounce (nothing). A second uniform random number ϕ'_α determines the outcome:

$$\text{dynamic}_\alpha = \begin{cases} \text{coalescence}, & \phi'_\alpha \leq E_c(\mathbf{a}_j, \mathbf{a}_k) \\ \text{breakup}, & E_c(\mathbf{a}_j, \mathbf{a}_k) < \phi'_\alpha \leq E_b(\mathbf{a}_j, \mathbf{a}_k)(1 - E_c(\mathbf{a}_j, \mathbf{a}_k)) + E_c(\mathbf{a}_j, \mathbf{a}_k) \\ \text{bounce}, & \phi'_\alpha > E_b(\mathbf{a}_j, \mathbf{a}_k)(1 - E_c(\mathbf{a}_j, \mathbf{a}_k)) + E_c(\mathbf{a}_j, \mathbf{a}_k) \end{cases} \tag{5}$$

https://doi.org/10.5194/egusphere-2022-1243
Preprint. Discussion started: 22 November 2022

Once the dynamic is determined, a fragment size is sampled if necessary:

4. Sample a fragment size $M_{f,\alpha}$ (mass) from a fragment size distribution, $P_{f,\alpha}$, with cumulative distribution function (CDF) $C_{f,\alpha}(\phi)$ that depends on the colliding particle attributes. A related variable, $N_{f,\alpha}$, is taken to denote the number of fragments that would form in a collision between droplets of mass M_j and M_k: $N_{f,\alpha} = \frac{M_k + M_j}{M_{f,\alpha}}$.

Finally, updating of multiplicities and attributes proceeds based on the selected dynamic, number of collisions, and sampled fragment size (if applicable):

https://doi.org/10.5194/egusphere-2022-1243
Preprint. Discussion started: 22 November 2022

(a) For coalescence:

$$\begin{cases} \xi_j' = \xi_j - \gamma_\alpha \xi_k \\ \mathbf{a}_k' = \mathbf{a}_k + \gamma_\alpha \mathbf{a}_j \\ \text{if } \xi_j = 0, \text{ then } \xi_j', \xi_k' = \xi_k/2,\ \mathbf{a}_j' = \mathbf{a}_k \end{cases} \tag{6}$$

The coalescence rate is incremented by $\gamma_\alpha \xi_k$.

(b) For breakup:

In some cases, only $\gamma_{jk} \leq \gamma_\alpha$ breakups can occur for a given superdroplet pair without encountering negative multiplicities. We compute this maximum possible number of breakup steps and update the superdroplet properties using a recurrence relation (assuming $\gamma_\alpha > 0$), and track a breakup deficit rate of $\gamma_\alpha - \gamma_{jk}$. (Alternatively, one may perform substepping of the breakup event.) The particle attributes are updated such to be consistent with the result of several breakup steps with $\gamma_\alpha = 1$ occurring in sequence, always producing fragments of size $M_{f,\alpha}$.

$$\begin{cases} \gamma_{jk} = 0 \\ \xi_j^{\text{transfer}} = \xi_k \\ \xi_k^{\text{new}} = 0 \\ \text{while } \gamma_{jk} < \gamma_\alpha \quad \text{and} \quad \xi_j^{\text{transfer}} < \xi_j: \\ \qquad \xi_j^{\text{transfer}} = \xi_j^{\text{transfer}} + \xi_k^{\text{new}} \\ \qquad \xi_k^{\text{new}} = \xi_k^{\text{new}} \left(\frac{M_j}{M_{f,\alpha}} \right) + \xi_k \frac{M_j + M_k}{M_{f,\alpha}} \\ \qquad \gamma_{jk} = \gamma_{jk} + 1 \end{cases} \tag{7}$$

$$\begin{cases} \xi_j' = \xi_j - \xi_j^{\text{transfer}} \\ \xi_k' = \xi_k^{\text{new}} \\ \mathbf{a}_k' = \frac{\xi_k \mathbf{a}_k + \xi_j^{\text{transfer}} \mathbf{a}_j}{\xi_k^{\text{new}}} \\ \text{if } \xi_j = 0, \text{ then } \xi_j', \xi_k' = \xi_k/2,\ \mathbf{a}_j' = \mathbf{a}_k \end{cases} \tag{8}$$

The breakup rate is incremented by $\gamma_{jk} \xi_k$. The breakup deficit rate is incremented by $(\gamma_\alpha - \gamma_{jk}) \xi_k$

(c) For bounce:

No update is made to droplet multiplicities or attributes, and only the collision counter is incremented.

https://doi.org/10.5194/egusphere-2022-1243
Preprint. Discussion started: 22 November 2022

2.3 Additional Implementation Details

This method of breakup allows for the splitting of a coalesced transition state into a non-integer number of fragments ($N_{f,\alpha} = \frac{M_k+M_j}{M_{f,\alpha}}$ need not be integer), depending on the sampled fragment size. For instances where it may be desirable to preserve superdroplet multiplicities as integers, we recommend rescaling the multiplicities after the breakup step by a factor of $r_k = \lceil \xi_k \rceil / \xi_k$, and the multiplicities correspondingly by $1/r_k$ such that extensive attributes (including mass) are conserved.

The presence of a "breakup deficit" in the case where $\gamma_{jk} < \gamma_\alpha$ can be averted by substepping, though this is inadvisable for highly parallel applications of the SDM. Furthermore, superdroplet multiplicities may increase without bound according to the algorithm as presented above, which can lead to numerical artifacts and instability within a simulation. A set of limiters preventing runaway multiplicity is discussed in Appendix A. Finally, a method for sampling a fragment size from a highly nonlinear empirical distribution, such as Straub 2010, is discussed in Appendix B.

3 Numerical Experiments and Discussion

To demonstrate the behavior and impact of the proposed breakup algorithm on particle size spectra and process rates, we present a set of zero-dimensional box and one-dimensional rainshaft cases that include collisional breakup, implemented in the open-source Pythonic superdroplet code 'PySDM' (Bartman et al., 2022b). All simulations use a geometric collision kernel, where the rate of collisions K_{jk} between droplets with the properties of superdroplets j and k is given by

$$K_{jk} = \pi (R_j + R_k)^2 |v_j - v_k| \tag{9}$$

where R_j is the radius of particle j and v_j is the terminal velocity/fall speed of particle j, computed using the parameterization of Gunn and Kinzer. Collisions within a superdroplet (i.e. collisions between droplets represented by the same superdroplet) are not considered in 'PySDM', though the use of a geometric collision kernel results in zero collisions between equally-sized droplets, as they have the same terminal velocity.

The coalescence efficiency is specified to be either a constant value (for sensitivity studies), or the empirical coalescence efficiency of Straub et al. which depends on the Weber number of the colliding droplet pair. (The Weber number is a ratio of kinetic collisional energy and surface tension, and relates to the stability of a droplet pair under collision.) We consider three types of fragmentation functions: (1) a constant fragment number N_f, in which the particle-size distribution (PSD) is a delta function $P_f(M_{f,\alpha}) = \delta(M_{f,\alpha} - \frac{M_j+M_k}{N_f})$; (2) a normal distribution $M_{f,\alpha} \sim \mathcal{N}(\mu, \sigma)$ where the mean μ and variance σ^2 are specified; and (3) the empirically derived fragmentation function of Straub et al., which uses four categories of fragmentation and lognormal or normal subdistributions.

3.1 Particle Size Distribution

The zero-dimensional box simulations include collisional-coalescence and breakup dynamics only. The droplet size distribution is initialized to an exponential distribution in mass x, given by $N(x) = x_0 \exp(-x/x_0)$ with the characteristic size $x_0 = (4\pi/3)R_0^3$ set using $R_0 = 30.531 \mu\mathrm{m}$ as in Shima et al. (2009). The simulations employ $2^{13} = 8192$ superdroplets to represent

https://doi.org/10.5194/egusphere-2022-1243
Preprint. Discussion started: 22 November 2022

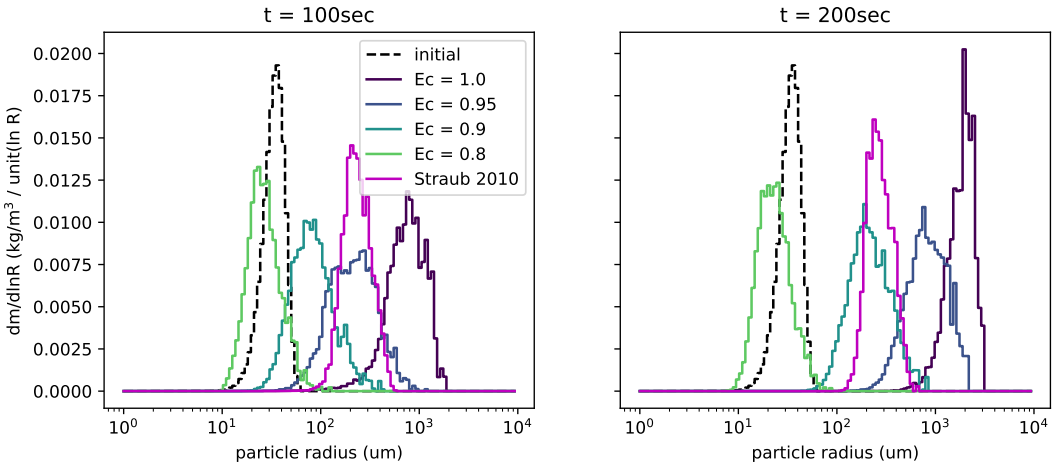

Figure 3. Particle size distribution with varying coalescence efficiencies under a geometric collision kernel after 100s (left) and 200s (right). The breakup fragmentation function is deterministic, with the fragment size determined as 1/8th the sum of the colliding droplet sizes. The dashed black line represents the initial PSD, and solid lines represent various fixed values of the coalescence efficiency. The pink line corresponds to a size-dependent coalescence efficiency from Straub et al..

a number density of $100/\mathrm{cm}^3$ in a box of volume $1\mathrm{m}^3$ with a fixed time step of $1\mathrm{s}$. This choice of superdroplet quantity is sufficient to produce consistent results in the PSD across realizations using a different random seed, and was shown by Shima et al. to closely match the exact PSD in a similar box model simulation of collisional coalescence. All particle size distributions are displayed as the marginal mass distribution $g(R) = \frac{dm}{dln(R)} = 3x^2n(x)$ where $n(x)$ is the particle size distribution. This mass distribution is computed by binning the resulting superdroplets into 128 logarithmically-spaced size bins between particle radius $1\mu\mathrm{m}$ and radius $10\mathrm{mm}$. We separate the simulations into those which use a deterministic fragmentation function, in which breakups result in a constant number of fragments in any given collision; a stochastic fragmentation function with fragment sizes sampled from a specific distribution; and a size-dependent fragmentation function, where the fragment sizes are sampled from a distribution whose parameters depend on the colliding particles. We further include experiments exploring the use of a fixed coalescence efficiency versus a particle-attribute-derived coalescence efficiency. This separation elucidates which aspects of the particle population behavior are attributable to stochastic stochastic sampling of the fragmentation function, or related to particle-property-dependent parameters such as Weber number.

3.1.1 Deterministic and Size Independent Fragmentation

First we investigate the sensitivity of the PSD evolution to the coalescence efficiency, using four values of a constant-valued efficiency E_c between 0.8 and 1.0 ($E_c = 1.0$ corresponds to coalescence-only) and a particle-size dependent E_c parameterization (Straub et al., 2010). All simulations use a deterministic fragmentation function in which all single-step collisional breakups

https://doi.org/10.5194/egusphere-2022-1243
Preprint. Discussion started: 22 November 2022

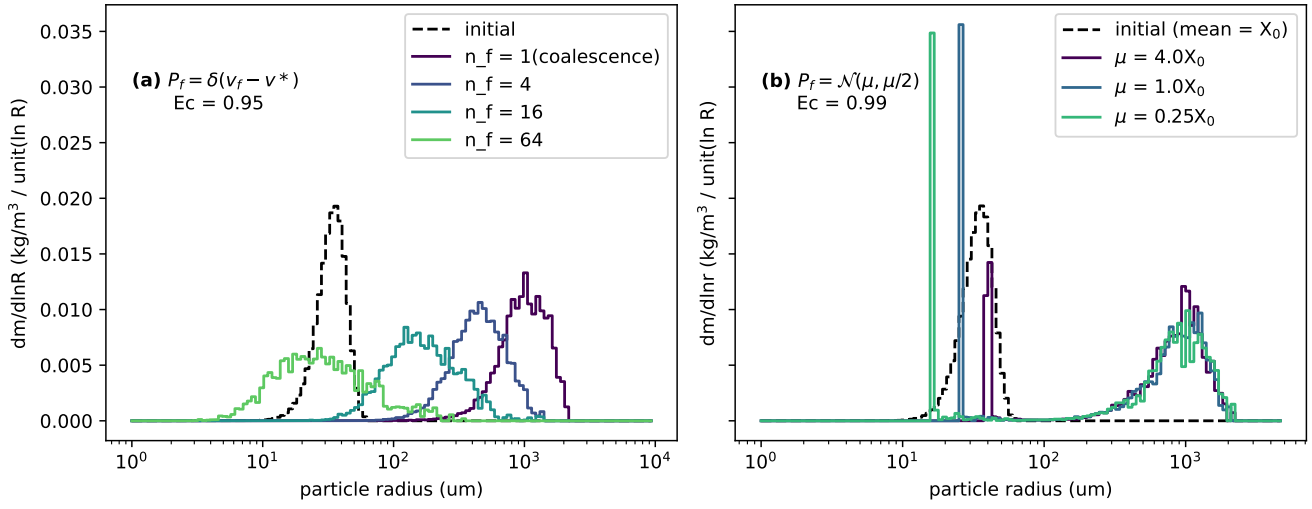

Figure 4. Sensitivity to fragmentation function of PSDs following collisions with a geometric kernel and fixed coalescence efficiency in a deterministic and stochastic fragmentation function case. (Left) The fragment size is fixed by a divisor of the sum of colliding particle volumes; (right) fragment size is sampled from a Gaussian distribution with varying means μ determined as a multiple of the initial distribution mean, with variance $\sigma^2 = \mu^2/4$. The initial distribution is shown as a black dashed line in each figure.

result in $N_f = 8$ fragments:

$$P_{f,\alpha}(M_f) = \delta\big(M_f - \frac{M_j + M_k}{N_f}\big). \tag{10}$$

Figure 3 displays two snapshots of the PSD under this set of dynamics, demonstrating the impact of stochasticity in selecting whether coalescence or breakup occurs, independent of sampling a fragment size. As expected, the initial PSD broadens and shifts toward larger droplets at 100s, with the largest values of fixed E_c leading to the largest increase in average particle mass. However, after 200s, the PSD for the $E_c = 0.8$ case remains approximately steady with a mean size that is smaller than the initial distribution mean, demonstrating that coalescence and breakup are approximately balanced in this case.

By contrast, the PSD for the Straub 2010 parameterization of E_c is initially comparable to the $E_c = 0.95$ simulation at 100s, but narrows without shifting toward much larger droplets after further time has elapsed, leading to a dominant mode that is more similar to the $E_c = 0.9$ case. This empirical parameterization also shows evidence of approaching a steady state distribution, in which coalescence and breakup rates are matched on average, driving the PSD to a stationary state. The Straub 2010 parameterization decreases exponentially with the colliding particle Weber number, which is correlated with the size and relative velocity of the colliding particles. Two colliding particles with a similar size have a low relative velocity, therefore as the PSD shifts toward larger coalesced droplets, there is a competing effect between a larger particle size increasing the Weber number, and decreased relative velocity reducing it. This competition produces the stationary behavior and narrowing of the PSD observed in this case.

https://doi.org/10.5194/egusphere-2022-1243
Preprint. Discussion started: 22 November 2022

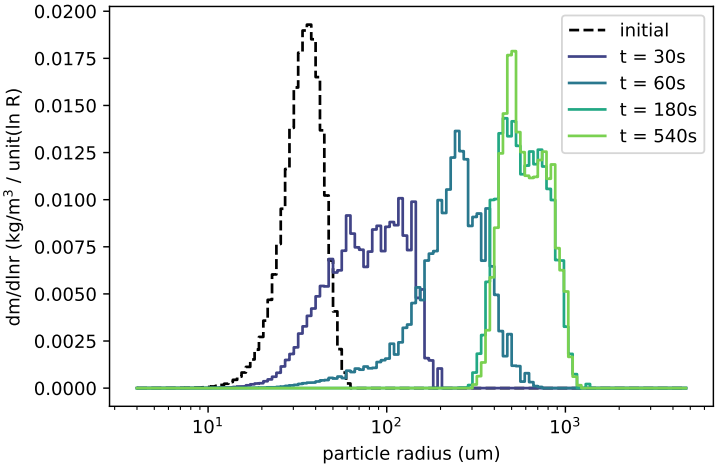

Figure 5. Initial PSD (black dashed) and PSD's following collisions with a geometric kernel, the Straub 2010 collection efficiency, and the Straub 2010 fragmentation function Straub et al. (2010) after several elapsed times (colors).

Next we consider the PSD evolution when the coalescence efficiency is held fixed at a constant value and the fragmentation function is varied. In figure 4(a), we consider a deterministic fragmentation function where the number of fragments from a single breakup event is fixed (as in figure 3), as well as a Gaussian fragment size distribution with mean μ specified as a multiple of the initial mean particle mass x_0, and variance $\sigma^2 = \mu^2/4$. When the number of fragments is fixed, results using the largest number of fragments display the smallest mean particle size and broadest spectra. The first behavior is expected, as a larger value of N_f results in smaller typical fragment sizes. The broadening of the spectrum can be attributed to a wider range of collision rates between very small droplets (which result from fragmentation), and is generally an expected outcome of including collisional breakup.

When the fragment size is sampled from a normal distribution (figure 4(b)), the resulting spectra are bimodal, with a large-droplet mode that is similar between different choices of the mean μ, and a narrow small-droplet mode that depends on the distribution parameters. The appearance of a second mode occurs when the fragment size is sampled from the left tail of the fragment size distribution, whereas the large mode corresponds to a droplets undergoing coalescence only, as in the $N_f = 1$ case. This behavior indicates that through stochastic sampling of the dynamic and fragment size together, the droplet population splits into one mode which fragments into smaller droplets, and a second mode which primarily undergoes coalescence and grows in size. Because larger droplets collide at much quicker rates than small droplets, the fragmented mode is less likely to collide and re-coalesce to form medium-sized droplets, while the coalesced-mode retains some probability of colliding and either growing (coalescing), or breaking up into smaller droplets. Thus we observe that the small-droplet-mode grows in this instance, with particles effectively become "stuck" in this dynamical regime due to the separation of scales in collision rates.

https://doi.org/10.5194/egusphere-2022-1243
Preprint. Discussion started: 22 November 2022

3.1.2 Stochastic Size-Dependent Fragmentation

Finally, we consider an empirically derived coalescence efficiency (Straub et al., 2010, as above) in conjunction with a complex empirical fragmentation function whose parameters depend on the colliding droplet properties. In figure 5, we consider the evolution of the PSD under the Straub 2010 efficiency and fragmentation dynamics, beginning from the same initial distribution as previous experiments. At first, the PSD broadens and shifts towards larger droplet sizes, as in figure 3, but the PSD after 540s is virtually unchanged from the PSD at 180s. These results indicate the stationarity of the particle size distribution after sufficient time has elapsed: coalescence and breakup are balanced, as in the previous example. Contrasted with figure 3, which used a deterministic size-independent fragmentation function, the stationary PSD resulting from the Straub et al. (2010) parameterization of fragmentation is broader and less symmetric. This difference reflects the use of sampling from a distribution of fragment sizes, contrasting with the symmetric PSDs found from using a fixed number of fragments.

3.2 Cloud and Precipitation Properties

Next we consider the impact of collisional breakup in a one-dimensional warm rain setting that includes condensation/evaporation (including aerosol activation/deactivation), collisions, and transport of particles within the column through advection and sedimentation/precipitation. These 1D simulations are based on the kinematic framework of Shipway and Hill, using a fixed profile of dry-air potential temperature and dry-air density $\rho_d(z)$, and a resolved budget of water vapor (advection and coupling with vapor uptake and release by particles). The vapor advection is solved using the MPDATA algorithm on a columnar grid with spatial grid step of $25\mathrm{m}$ (employing the PyMPDATA implementation Bartman et al., 2022a). An aerosol population with hygroscopicity $\kappa = 0.9$ is initialized throughout the vertical domain with $2^{10} = 1024$ superdroplets per gridbox. This choice of 1024 superdroplets per gridbox reflects the higher computational demands of the one dimensional simulation compared to the box model, and still produces statistically convergent results in the mesoscale quantities investigated across simulation instances. For the first 600s of spin-up, condensation-evaporation (including aerosol activation) and particle advection are the only active dynamics, with a time-varying updraft momentum flux of $\rho_d w(t) = 3\mathrm{kgm}^{-3}\mathrm{ms}^{-1}\sin(\pi t/600\mathrm{s})$. After this spin-up time, the updraft velocity is set to 0, particle displacement due to sedimentation is enabled, and collision-coalescence-breakup is allowed to occur. The time step is fixed at $1\mathrm{s}$ throughout the simulation.

The test cases demonstrated here include a no-breakup case, a property-independent breakup case where the coalescence efficiency is fixed and fragment sizes are sampled from a fixed distribution, and the particle-property-dependent empirical coalescence efficiency and fragmentation parameterizations from Straub et al.. All simulations use a geometric collision rate (equation 9) and the Gunn and Kinzer terminal velocity parameterization. In the no-breakup case, all collisions result in coalescence. In the property-independent breakup case, we fix $E_c = 0.95$ for all superdroplet collisions based on the correspondence in figure 3 to the empirical coalescence efficiency. This case samples fragment sizes from a Gaussian distribution in particle volume with mean radius $30\mu\mathrm{m}$ and standard deviation $15\mu\mathrm{m}$. In contrast to the property-independent case, in which the fragmentation parameters are hand-selected, the property-dependent setting is based on empirical evidence, and is expected to be more reflective of the variability of real clouds. In both the property-independent and -dependent cases, the breakup efficiency

https://doi.org/10.5194/egusphere-2022-1243
Preprint. Discussion started: 22 November 2022

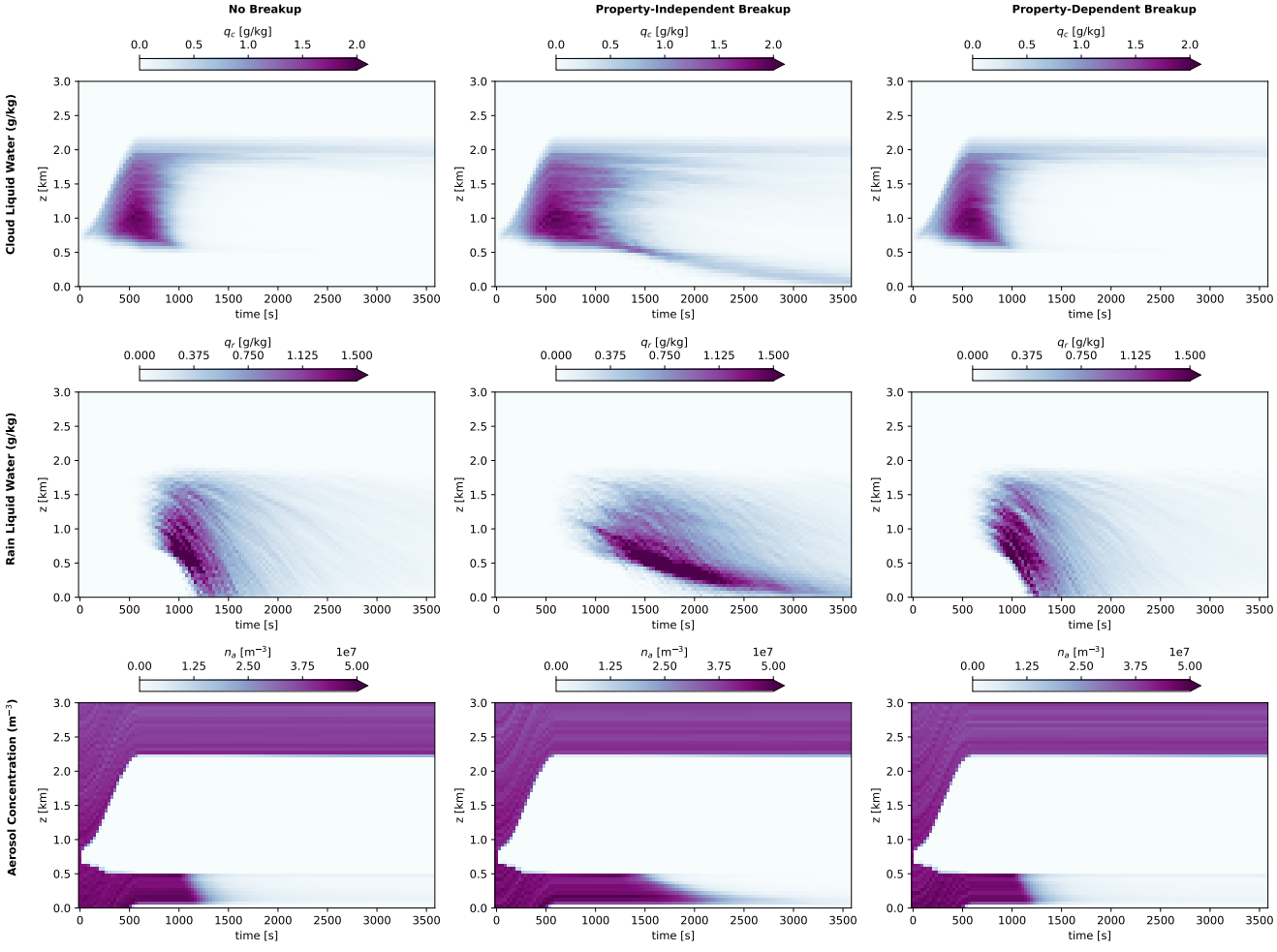

Figure 6. Hydrometeor concentrations without breakup (left column), with breakup using a property-independent coalescence efficiency (middle column), and with breakup following the property-dependent Straub et al. (2010) parameterizations (right column). Included are cloud water mixing ratio (top row), rain water mixing ratio (middle row), and aerosol number concentration (bottom row).

is set to $E_b = 1$ such that all collisions result in either coalescence or breakup. To contrast the behavior of the three cases, we consider the hydrometeor population at various altitudes throughout the simulation, as well as collision process rates and aerosol processing rates.

3.2.1 Hydrometeor and Cloud Quantities

The mixing ratio of cloud droplets (activated droplets of no more than $50\mu m$ radius), rain droplets (radius greater than $50\mu m$), and the number concentration of unactivated aerosols are displayed for the three test cases in figure 6. The no-breakup simulation forms a cloud due to activation of aerosols between 500m and 2200m altitude until the updraft is terminated after 600s.

https://doi.org/10.5194/egusphere-2022-1243
Preprint. Discussion started: 22 November 2022

Larger rain-range droplets form from collisional coalescence and begin to sediment out of the system in clusters, visible as distinct streaks in the (t, z) plane, with surface precipitation beginning around 1200s into the simulation, depleting the cloud droplet population.

When property-independent breakup is included, a higher concentration of cloud-sized droplets persists at cloud base, and the surface precipitation is delayed and spread out relative to the case with no breakup. This behavior indicates that rain droplets favorably break up within the cloud and especially near cloud base, fragmenting into smaller cloud droplets (the mean of the fragment size distribution is $30\mu\mathrm{m}$ radius, only slightly lower than the rain size range) with a lower sedimentation rate. Furthermore, the aerosol population below cloud base is not depleted as quickly in this property-independent case, indicating a reduction in aerosol scavenging and washout that is consistent with the lower precipitation rates. These phenomena are consistent with documented impacts of collisional breakup such as suppressed surface precipitation (Seifert et al., 2005), and show that the proposed algorithm can meaningfully represent the breakup process.

The empirical property-dependent breakup case using the Straub et al. parameterizations displays hydrometeor populations that are more similar to the no-breakup case, indicating that the choice of $E_c = 0.95$ in the property-independent case likely overestimates the rate of collisional breakup when condensation and evaporation are present (contrasted with figure 3). As in the no-breakup case, the property-dependent empirical case displays distinct streaks of precipitation, with surface precipitation initiated around 1200s.

The $3\mathrm{m/s}$ updraft velocity used in this setup leads to a relatively shallow cloud, with drizzle-range precipitable hydrometeors which are less likely to undergo collisional breakup than very large droplets in a deeper convective setting. The likelihood of breakup in the Straub parameterization is strongly correlated with the size of the colliding droplets, therefore we expect to see a stronger impact of including SDM breakup in a strongly precipitating convective case. Due to challenges and complexity of representing mixed-phase hydrometeors in the superdroplet method, we do not present any such deep convective experiment. However, it has been noted that collisional breakup of supercooled liquid droplets upon impact with ice is a potentially important secondary ice production mechanism (Zhao and Liu, 2022; James et al., 2021; Phillips et al., 2018), thus we suggest that the novel SDM breakup representation presented in this work could be an instrumental tool in further research on secondary ice production and mixed-phase processes.

3.2.2 Process Rates

Figure 7 displays the local rates of superdroplet collision (scaled by multiplicity), as well as distinguishing between rates of coalescence and rates of breakup. We see an expected correlation between the time and location of collisions in all three cases with the location of hydrometeors (outlined in black for cloud and red for rain)–as expected, a higher concentration of hydrometeors, particularly large rain-range hydrometeors corresponds to higher rates of all collisional dynamics. The rate of collisions increases throughout the simulation time, particularly near cloud base where the largest droplets are sedimenting and colliding at higher rates. The property-independent case is consistent with the other cases in displaying higher collision rates at cloud base, even though the droplets in this region are slightly smaller and fall in the cloud category.

https://doi.org/10.5194/egusphere-2022-1243
Preprint. Discussion started: 22 November 2022

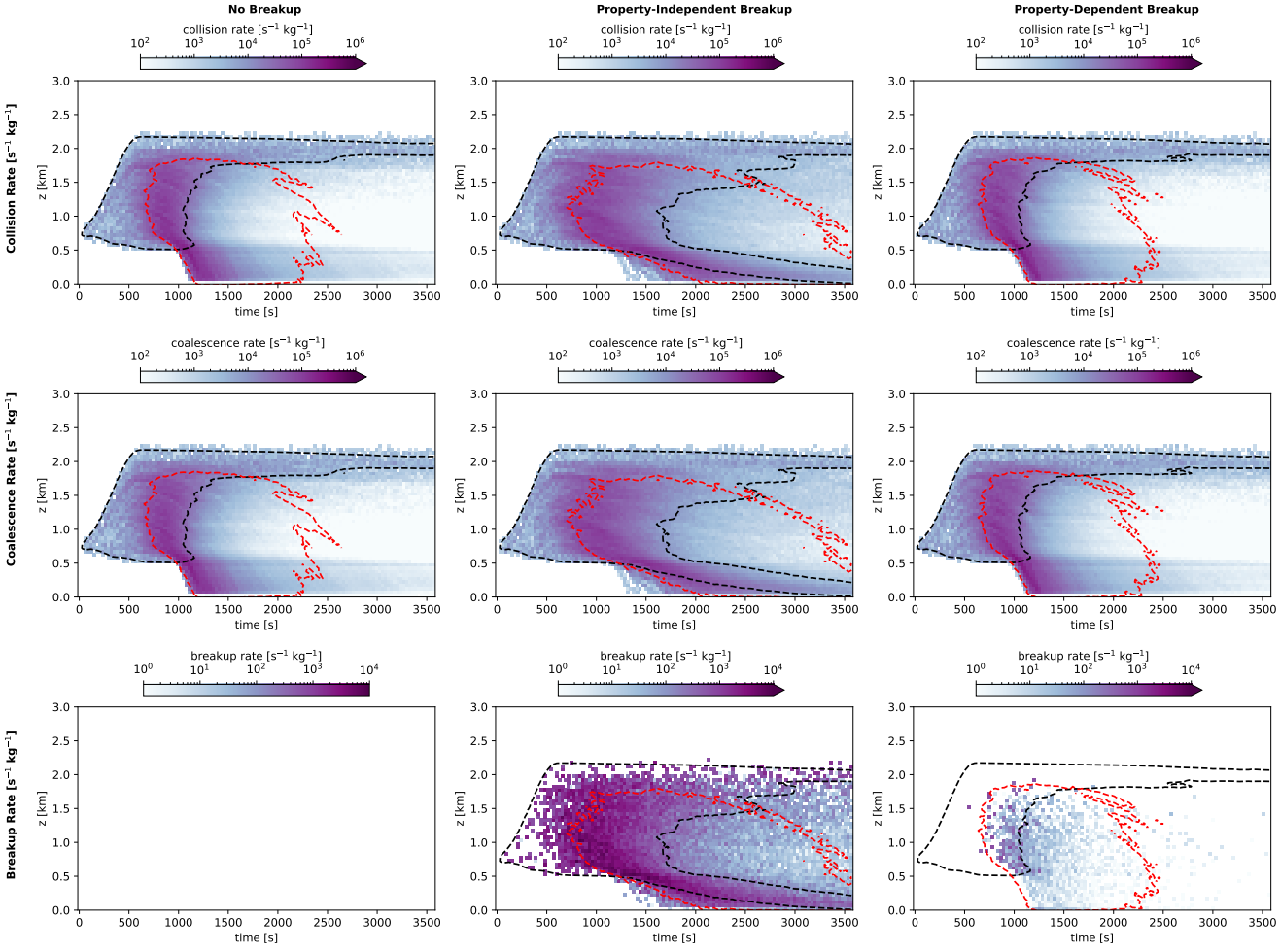

Figure 7. Collisional dynamic rates for the 1-dimensional case with (left) no breakup, (middle) breakup with a fixed coalescence efficiency, and (right) breakup with the Straub 2010 parameterizations. The dynamics shown include (top to bottom): collision rate, coalescence rate, and breakup rate. Dashed contour lines represent the level of $q_c = 0.2\text{g/kg}$ (black) and $q_r = 0.2\text{g/kg}$ (red), representing a cloudy and rainy region of the time-space domain, respectively.

https://doi.org/10.5194/egusphere-2022-1243
Preprint. Discussion started: 22 November 2022

All three cases display similar rates of collision and coalescence, with the highest of these rates occurring in the cloud among rain droplets, and below cloud base among precipitating rain droplets. In the no-breakup case, every feasible collision results in a coalescence, and the breakup rate is zero. When property-independent breakup is included, the time-space distribution of the breakup rate is nearly identical to that of the collision rate. This trend is consistent with the use of a uniform coalescence efficiency $E_c = 0.95$, which is agnostic to the size of the colliding particles. In contrast, the empirical property-dependent case sees collisional breakup primarily where larger rain droplets are present, consistent with the Straub et al. parameterization based on Weber number. In this case, breakup events are much less frequent, and thus breakup plays less of a role in determining the hydrometeor populations of this simulation case. These results demonstrate that the SDM breakup algorithm can produce expected process behavior in both a property-independent setting, where the collision dynamics result in strong breakup, and in an empirically parameterized setting.

As noted in the discussion of figure 6, the property-independent breakup case experiences a persistent population of aerosols below cloud base, while the no-breakup and property-dependent cases demonstrate washout upon the onset of precipitation. Collision breakup resulting in very small droplet fragments could potentially introduce cloud droplets so small that they deactivate in their environment. In figure 8, we investigate differences in aerosol processing rates under these collisional breakup scenarios, looking at rates of aerosol activation, deactivation, and ripening.

The property-independent and no-breakup cases have nearly identical behavior in aerosol processing, consistent with the correspondence between their hydrometeor concentrations and collision process rates. In all three cases, a few superdroplets at cloud top encounter humidity close to their critical supersaturation, which results in the "ripening" processes of fluctuation between an activated and deactivated state due to competition when the supersaturation is insufficient to activate all aerosols (e.g., Arenberg, 1939; Wood et al., 2002). (We define ripening rate as the number of activated droplets growing through condensation per unit of time within a grid cell in which deactivation simultaneously occurs on other particles). Several instances of ripening occur within the extended cloud base of the property-dependent case, indicating that breakup events in this time-space domain produce fragments whose critical supersaturation is close to the environment supersaturation (i.e., hinting breakup-induced deactivation, conceptually analogous to collision-induced activation discussed in Hoffmann, 2017). Aerosols activate primarily at the start of the simulation when an updraft is present, defining the altitude boundaries of the cloud. No additional activation is seen in either instance including collisional breakup. Deactivation occurs among a few aerosols which activate and then rise in altitude beyond cloud top initially, and more strongly below cloud base as droplets sediment out of the cloud and evaporate. The property-independent case experiences much stronger deactivation at cloud base, which corresponds to the higher rate of fragmentation of droplets at this altitude.

The more realistic property-dependent case shows a close match in aerosol processing rates to the no-breakup case, indicating that collisional breakup is not a significant process for shallow clouds such as this kinematic one-dimensional setting. However, the enhanced rates of ripening and deactivation in the property-independent case indicate that collisional breakup could be a relevant process for future studies of aerosol-cloud effects, particularly in deeper-convective cases where collision rates are likely to be higher. The SDM representation of collisional breakup presented in this work can capture such potential effects, making it a useful tool for future studies of microphysics processes.

https://doi.org/10.5194/egusphere-2022-1243
Preprint. Discussion started: 22 November 2022

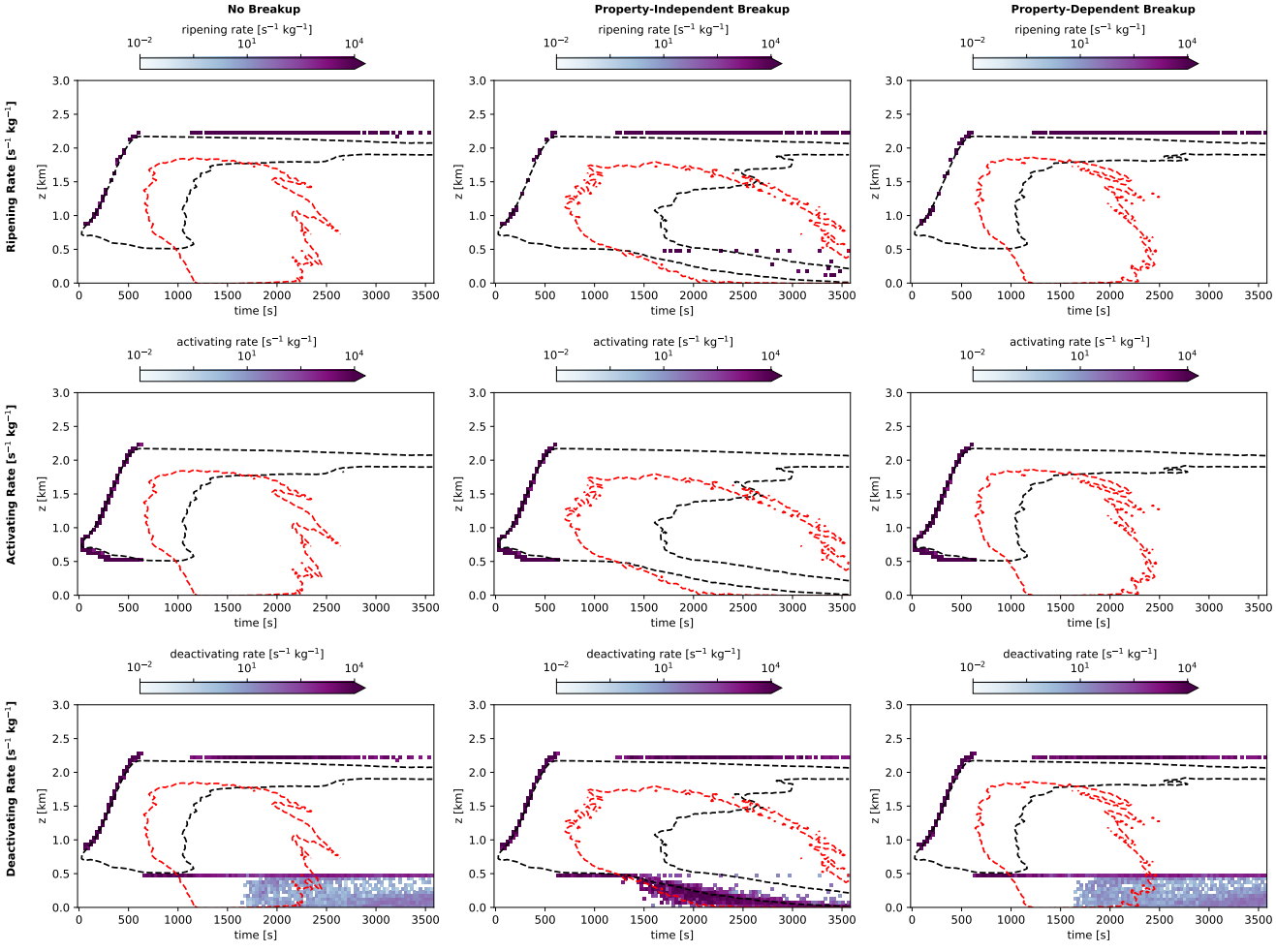

Figure 8. Aerosol processing rates for (left to right) no breakup, property-independent breakup, and Straub et al. (2010) parameterizations. Included are (top to bottom): ripening rate, activating rate, and deactivating rate. Dashed contour lines represent the level of $q_c = 0.2\mathrm{g/kg}$ (black) and $q_r = 0.2\mathrm{g/kg}$ (red), representing a cloudy and rainy region of the time-space domain, respectively.

https://doi.org/10.5194/egusphere-2022-1243
Preprint. Discussion started: 22 November 2022

4 Conclusions

This work presents a superdroplet algorithm for collisional breakup that is both scalable in avoiding creation of new superdroplets, and physical in its ability to produce results in a box and one-dimensional setting that are consistent with the expected suppression of rain. Furthermore, the algorithm produces hydrometeor populations and process rates that differ between a property-independent approach (with a fixed coalescence efficiency and fixed fragment size distribution), and a property-dependent approach using empirical parameterizations. These differences indicate the importance of random, stochastic events in warm rain microphysics, a trait which has also been documented in other microphysical phenomena such as giant CCN (Feingold et al., 1999; Yin et al., 2000). Without such a scalable representation, the superdroplet method has heretofore been unable to capture these additional stochastic impacts of breakup, nor has it been applied to compare empirical parameterizations of coalescence and breakup, which contribute uncertainties to operational process, weather, and climate models.

This work provides the basis for a more complete representation of microphysical processes in particle-based simulations. For instance, when combined with collisional breakup, a superdroplet representation of ice-phase hydrometeors could probe processes of secondary ice production. For instance, when supercooled water droplets collide with solid phase hydrometeors, they could break up, with small fragments freezing following impact or freezing onto the surface of the colliding ice crystal (Phillips et al., 2018; James et al., 2021). Similarly, collisional breakups between two ice crystals can lead to splintering and the formation of many smaller ice crystals, which then grow by vapor deposition (Harris-Hobbs and Cooper, 1987). These and other mixed-phase processes are poorly understood due to challenges in obtaining direct observational or laboratory measurements, thus a high-fidelity particle-based representation such as the superdroplet method provides an ideal means for studying these phenomena. While the collisional breakup representation presented here does not address underlying uncertainties in parameterization of processes such as collision rates and phase change, it provides a path forward for more rigorous and complete studies of cloud microphysics.

Code and data availability. Implementation of this breakup algorithm in the SDM is available at https://doi.org/10.5281/zenodo.7306034. The simulations presented in this work (and all necessary input information) are available in the folder 'deJong_Mackay_2022' at https://doi.org/10.5281/zenodo.7308668. The notebooks in this folder reproduce all results and figures presented in this study, with no external datasets required. The scripts run the relevant model configuration in a matter of minutes and plot the resulting output. All results presented in this paper can be reproduced by one of two means: (1) downloading and installing 'PySDM' and 'PySDM-examples' (e.g. using 'pip install'), and running the notebooks locally; (2) accessing the PySDM-examples repository online and running the examples notebooks in the folder 'deJong_Mackay_2022' on Google Colab. These codes, PySDM and PySDM-examples, are continuously under development at https://github.com/atmos-cloud-sim-uj/PySDM and https://github.com/atmos-cloud-sim-uj/PySDM-examples, and are further documented in a software publication (Arabas et al., 2022).

https://doi.org/10.5194/egusphere-2022-1243
Preprint. Discussion started: 22 November 2022

Appendix A: Limiters

In implementing collisional breakup for superdroplets, we suggest imposing a few limiters to enforce physical constraints and maintain stability of the code. If the user-selected time step for the SDM implementation is too large, collisional breakup may quickly become a runaway process with superdroplet multiplicities increasingly rapidly and unphysically, leading to numerical overflow. As an example, suppose a droplet of multiplicity 10^2 should undergo 6 collisional breakups ($\gamma_\alpha = 5$) into 5 fragments each time ($N_{f,\alpha} = 5$): then $\gamma_{jk} = 3906$ and its new multiplicity is $15,525 = \mathcal{O}(10^4)$. Successive collisional breakups between droplets whose multiplicities have grown so rapidly would then lead to exponentially booming multiplicities, and could quickly exceed the maximum representable quantity for the computing machine (overflow). One solution is to set a maximum allowable multiplicity for any superdroplet, and to reject any collisional breakups that would produce a superdroplet exceeding this multiplicity.

In addition, the process of collisional breakup is physically constrained such that the resulting superdroplet (the "fragment“) volume should not exceed the volume of either colliding droplets, nor should it drop below a realistic size for a liquid water droplet (molecule scale, for instance). These physical constraints can be imposed by setting a minimum and maximum allowable fragment size resulting from breakup.

The first of these constraints can then be imposed during computation of γ_{jk} within the while loop in equation 7:

$$\xi_k^{\mathrm{new}} \leq \xi_{\max} \tag{A1}$$

where $\xi_{\max}$ is a maximum multiplicity set to prevent overflow. The second two constraints are imposed during the sampling of a fragment size:

$$M_{\min} \leq M_{f,\alpha} \leq \max(M_j, M_k) \tag{A2}$$

where $M_{\min}$ is a minimum physically allowed fragment size, and the final constraint restricts the resulting fragment to be no larger than either colliding droplet.

Appendix B: Sampling from empirical fragment size distributions

Sampling a fragment size $M_{f,\alpha}$ requires the CDF of the fragment size distribution $P_f(\phi)$, which can be challenging for an empirical fragmentation function that is piecewise and lacks a closed form CDF. For instance, the commonly-used fragmentation function of Low and List partitions the fragment size distribution into three categories of distinct functional form, corresponding to filament, sheet, and disk breakup. Similarly, Straub et al. distinguish four categories of fragmentation, with the fragment size distribution within each category following a lognormal or normal distribution. We will demonstrate how a uniform random number ϕ''_α can be used to sample a fragment size from such complex distributions, following the notation of Straub et al..

https://doi.org/10.5194/egusphere-2022-1243
Preprint. Discussion started: 22 November 2022

Suppose the unnormalized fragment size distribution $P_f(D)$ in droplet diameter D is described as a sum of k subdistributions:

$$P_f(D) = \sum_{r=1}^{k} N_r p_r(D) \tag{B1}$$

where N_r is the expected number of fragments from mode r, and $p_r(D)$ is the normalized fragment size distribution for mode r. Note that $\int_0^\infty P_f(D)dD = \sum_{r=1}^{k} N_r \neq 1$ is the expected total number of fragments, and thus sampling a fragment size from the distribution requires normalization.

To sample a single fragment size D_f, we first use the random number ϕ''_α to determine which mode of fragmentation occurs by finding s such that

$$\frac{\sum_{r=1}^{s-1} N_r}{\sum_{r=1}^{k} N_r} \leq \phi''_\alpha < \frac{\sum_{r=1}^{s} N_r}{\sum_{r=1}^{k} N_r}. \tag{B2}$$

The fragment size is then chosen by sampling at random from the CDF of $p_s(D)$, which is assumed to be approximable by a closed form equation (as in the case of a Gaussian or lognormal distribution). This second step of sampling can be accomplished by selecting a new random number, reusing the random number from a different colliding droplet pair, or simply rescaling ϕ''_α to the selected mode s:

$$\tilde{\phi}''_\alpha = \frac{\phi''_\alpha - \sum_{r=1}^{s-1} N_r}{\sum_{r=1}^{s} N_r - \sum_{r=1}^{s-1} N_r}. \tag{B3}$$

The fragment size D_f is then chosen such that

$$\tilde{\phi}''_\alpha = p_s(D_f). \tag{B4}$$

Author contributions. EdJ led the code development, generation of results, interpretation, and writing. BM contributed to code development and the underlying methodology. AJ contributed to underlying methodology and interpretation of results. SA contributed to the code development, interpretation, and leads maintenance of the PySDM codebase.

Competing interests. The authors declare there to be no competing interests present related to this work.

Acknowledgements. We thank Tapio Schneider and Shin-ichiro Shima for feedback, insights, and discussion. Additional thanks go to Piotr Bartman for ongoing support of PySDM and to Oleksii Bulenok for assistance in GPU backend and code review for the collisional breakup dynamics. E. de Jong was supported by a Department of Energy Computational Sciences Graduate Fellowship. S. Arabas acknowledges support from the Polish National Science Center (grant no. 2020/39/D/ST10/01220). This research was additionally supported by Eric and Wendy Schmidt (by recommendation of Schmidt Futures) and the Heising-Simons Foundation.

https://doi.org/10.5194/egusphere-2022-1243
Preprint. Discussion started: 22 November 2022

References

Andrejczuk, M., Reisner, J. M., Henson, B., Dubey, M. K., and Jeffery, C. A.: The potential impacts of pollution on a nondrizzling stratus deck: Does aerosol number matter more than type?, Journal of Geophysical Research: Atmospheres, 113, https://doi.org/10.1029/2007JD009445, 2008.

Andrejczuk, M., Grabowski, W. W., Reisner, J., and Gadian, A.: Cloud-aerosol interactions for boundary layer stratocumulus in the Lagrangian Cloud Model, Journal of Geophysical Research: Atmospheres, 115, https://doi.org/10.1029/2010JD014248, 2010.

Arabas, S., Bartman, P., Jong, E. d., Singer, C., Olesik, M. A., Mackay, B., Bulenok, O., Azimi, S., Górski, K., Jaruga, A., Piasecki, B., and Badger, C.: atmos-cloud-sim-uj/PySDM: PySDM v2.12, https://zenodo.org/record/7037182, 2022.

Arenberg, D.: Turbulence As The Major Factor in the Growth of Cloud Drops, Bulletin of the American Meteorological Society, 20, 444–448, https://doi.org/10.1175/1520-0477-20.10.444, 1939.

Barros, A. P., Prat, O. P., Shrestha, P., Testik, F. Y., and Bliven, L. F.: Revisiting Low and List (1982): Evaluation of Raindrop Collision Parameterizations Using Laboratory Observations and Modeling, Journal of the Atmospheric Sciences, 65, 2983–2993, https://doi.org/10.1175/2008JAS2630.1, 2008.

Bartman, P., Banaśkiewicz, J., Drenda, S., Manna, M., Olesik, M. A., Rozwoda, P., Sadowski, M., and Arabas, S.: PyMPDATA v1: Numba-accelerated implementation of MPDATA with examples in Python, Julia and Matlab, Journal of Open Source Software, 7, 3896, https://doi.org/10.21105/joss.03896, 2022a.

Bartman, P., Bulenok, O., Górski, K., Jaruga, A., Łazarski, G., Olesik, M. A., Piasecki, B., Singer, C. E., Talar, A., and Arabas, S.: PySDM v1: particle-based cloud modeling package for warm-rain microphysics and aqueous chemistry, Journal of Open Source Software, 7, 3219, https://doi.org/10.21105/joss.03219, 2022b.

Beard, K. V. and Ochs, H. T.: Collisions between Small Precipitation Drops. Part II: Formulas for Coalescence, Temporary Coalescence, and Satellites, Journal of the Atmospheric Sciences, 52, 3977–3996, https://doi.org/10.1175/1520-0469(1995)052<3977:CBSPDP>2.0.CO;2, 1995.

Berry, E. X.: Cloud Droplet Growth by Collection, Journal of Atmospheric Sciences, 24, 688–701, https://doi.org/10.1175/1520-0469(1967)024<0688:CDGBC>2.0.CO;2, 1967.

Bieli, M., Dunbar, O. R. A., de Jong, E. K., Jaruga, A., Schneider, T., and Bischoff, T.: An Efficient Bayesian Approach to Learning Droplet Collision Kernels: Proof of Concept Using "Cloudy," a New n-Moment Bulk Microphysics Scheme, Journal of Advances in Modeling Earth Systems, 14, e2022MS002 994, https://doi.org/10.1029/2022MS002994, 2022.

Chandrakar, K. K., Grabowski, W. W., Morrison, H., and Bryan, G. H.: Impact of Entrainment Mixing and Turbulent Fluctuations on Droplet Size Distributions in a Cumulus Cloud: An Investigation Using Lagrangian Microphysics with a Subgrid-Scale Model, Journal of the Atmospheric Sciences, 78, 2983–3005, https://doi.org/10.1175/JAS-D-20-0281.1, 2021.

Dziekan, P., Waruszewski, M., and Pawlowska, H.: University of Warsaw Lagrangian Cloud Model (UWLCM) 1.0: a modern large-eddy simulation tool for warm cloud modeling with Lagrangian microphysics, Geoscientific Model Development, 12, 2587–2606, https://doi.org/10.5194/gmd-12-2587-2019, 2019.

Feingold, G., Cotton, W. R., Kreidenweis, S. M., and Davis, J. T.: The Impact of Giant Cloud Condensation Nuclei on Drizzle Formation in Stratocumulus: Implications for Cloud Radiative Properties, Journal of the Atmospheric Sciences, 56, 4100–4117, https://doi.org/10.1175/1520-0469(1999)056<4100:TIOGCC>2.0.CO;2, 1999.

https://doi.org/10.5194/egusphere-2022-1243
Preprint. Discussion started: 22 November 2022

Grabowski, W. W.: Comparison of Eulerian Bin and Lagrangian Particle-Based Schemes in Simulations of Pi Chamber Dynamics and Microphysics, Journal of the Atmospheric Sciences, 77, 1151–1165, https://doi.org/10.1175/JAS-D-19-0216.1, 2020.

Grabowski, W. W., Morrison, H., Shima, S.-I., Abade, G. C., Dziekan, P., and Pawlowska, H.: Modeling of Cloud Microphysics: Can We Do Better?, Bulletin of the American Meteorological Society, 100, 655–672, https://doi.org/10.1175/BAMS-D-18-0005.1, 2019.

Gunn, R. and Kinzer, G. D.: The Terminal Velocity of Fall for Water Droplets in Stagnant Air, Journal of the Atmospheric Sciences, 6, 243–248, https://doi.org/10.1175/1520-0469(1949)006<0243:TTVOFF>2.0.CO;2, 1949.

Harris-Hobbs, R. L. and Cooper, W. A.: Field Evidence Supporting Quantitative Predictions of Secondary Ice Production Rates, Journal of the Atmospheric Sciences, 44, 1071–1082, https://doi.org/10.1175/1520-0469(1987)044<1071:FESQPO>2.0.CO;2, 1987.

Hoffmann, F.: On the limits of Köhler activation theory: how do collision and coalescence affect the activation of aerosols?, Atmospheric Chemistry and Physics, 17, 8343–8356, https://doi.org/https://doi.org/10.5194/acp-17-8343-2017, 2017.

James, R. L., Phillips, V. T. J., and Connolly, P. J.: Secondary ice production during the break-up of freezing water drops on impact with ice particles, Atmospheric Chemistry and Physics, 21, 18 519–18 530, https://doi.org/10.5194/acp-21-18519-2021, 2021.

Jensen, E. and Pfister, L.: Transport and freeze-drying in the tropical tropopause layer, Journal of Geophysical Research: Atmospheres, 109, https://doi.org/10.1029/2003JD004022, 2004.

Jokulsdottir, T. and Archer, D.: A stochastic, Lagrangian model of sinking biogenic aggregates in the ocean (SLAMS 1.0): model formulation, validation and sensitivity, Geoscientific Model Development, 9, 1455–1476, https://doi.org/10.5194/gmd-9-1455-2016, 2016.

Kamra, A. K., Bhalwankar, R. V., and Sathe, A. B.: Spontaneous breakup of charged and uncharged water drops freely suspended in a wind tunnel, Journal of Geophysical Research: Atmospheres, 96, 17 159–17 168, https://doi.org/10.1029/91JD01475, 1991.

Low, T. B. and List, R.: Collision, Coalescence and Breakup of Raindrops. Part I: Experimentally Established Coalescence Efficiencies and Fragment Size Distributions in Breakup, Journal of the Atmospheric Sciences, 39, 1591–1606, https://doi.org/10.1175/1520-0469(1982)039<1591:CCABOR>2.0.CO;2, 1982.

McFarquhar, G. M.: A New Representation of Collision-Induced Breakup of Raindrops and Its Implications for the Shapes of Raindrop Size Distributions, Journal of the Atmospheric Sciences, 61, 777–794, https://doi.org/10.1175/1520-0469(2004)061<0777:ANROCB>2.0.CO;2, 2004.

Morrison, H., Kumjian, M. R., Martinkus, C. P., Prat, O. P., and van Lier-Walqui, M.: A General N-Moment Normalization Method for Deriving Raindrop Size Distribution Scaling Relationships, Journal of Applied Meteorology and Climatology, 58, 247–267, https://doi.org/10.1175/JAMC-D-18-0060.1, 2019.

Morrison, H., Lier-Walqui, M. v., Fridlind, A. M., Grabowski, W. W., Harrington, J. Y., Hoose, C., Korolev, A., Kumjian, M. R., Milbrandt, J. A., Pawlowska, H., Posselt, D. J., Prat, O. P., Reimel, K. J., Shima, S.-I., Diedenhoven, B. v., and Xue, L.: Confronting the Challenge of Modeling Cloud and Precipitation Microphysics, Journal of Advances in Modeling Earth Systems, 12, https://doi.org/10.1029/2019MS001689, 2020.

Paoli, R., Hélie, J., and Poinsot, T.: Contrail formation in aircraft wakes, Journal of Fluid Mechanics, 502, 361–373, https://doi.org/10.1017/S0022112003007808, 2004.

Phillips, V. T. J., Patade, S., Gutierrez, J., and Bansemer, A.: Secondary Ice Production by Fragmentation of Freezing Drops: Formulation and Theory, Journal of the Atmospheric Sciences, 75, 3031–3070, https://doi.org/10.1175/JAS-D-17-0190.1, 2018.

Riechelmann, T., Noh, Y., and Raasch, S.: A new method for large-eddy simulations of clouds with Lagrangian droplets including the effects of turbulent collision, New Journal of Physics, 14, 065 008, https://doi.org/10.1088/1367-2630/14/6/065008, 2012.

Rogers, R. R. and Yau, M. K.: Short Course in Cloud Physics, Butterworth-Heinemann, 3 edn., 1989.

https://doi.org/10.5194/egusphere-2022-1243
Preprint. Discussion started: 22 November 2022

Schlottke, J., Straub, W., Beheng, K. D., Gomaa, H., and Weigand, B.: Numerical Investigation of Collision-Induced Breakup of Raindrops. Part I: Methodology and Dependencies on Collision Energy and Eccentricity, Journal of the Atmospheric Sciences, 67, 557–575, https://doi.org/10.1175/2009JAS3174.1, 2010.

Seifert, A. and Rasp, S.: Potential and Limitations of Machine Learning for Modeling Warm-Rain Cloud Microphysical Processes, Journal of Advances in Modeling Earth Systems, 12, e2020MS002 301, https://doi.org/https://doi.org/10.1029/2020MS002301, 2020.

Seifert, A., Khain, A., Blahak, U., and Beheng, K. D.: Possible Effects of Collisional Breakup on Mixed-Phase Deep Convection Simulated by a Spectral (Bin) Cloud Model, Journal of the Atmospheric Sciences, 62, 1917–1931, https://doi.org/10.1175/JAS3432.1, 2005.

Shima, S., Kusano, K., Kawano, A., Sugiyama, T., and Kawahara, S.: The super-droplet method for the numerical simulation of clouds and precipitation: a particle-based and probabilistic microphysics model coupled with a non-hydrostatic model, Quarterly Journal of the Royal Meteorological Society, 135, 1307–1320, https://doi.org/10.1002/qj.441, 2009.

Shima, S.-i., Sato, Y., Hashimoto, A., and Misumi, R.: Predicting the morphology of ice particles in deep convection using the super-droplet method: development and evaluation of SCALE-SDM 0.2.5-2.2.0, -2.2.1, and -2.2.2, Geoscientific Model Development, 13, 4107–4157, https://doi.org/10.5194/gmd-13-4107-2020, 2020.

Shipway, B. J. and Hill, A. A.: Diagnosis of systematic differences between multiple parametrizations of warm rain microphysics using a kinematic framework, Quarterly Journal of the Royal Meteorological Society, 138, 2196–2211, https://doi.org/10.1002/qj.1913, 2012.

Shirgaonkar, A. and Lele, S.: Large Eddy Simulation of Early Stage Contrails: Effect of Atmospheric Properties, in: 44th AIAA Aerospace Sciences Meeting and Exhibit, Aerospace Sciences Meetings, American Institute of Aeronautics and Astronautics, https://arc.aiaa.org/doi/10.2514/6.2006-1414, 2006.

Straub, W., Beheng, K. D., Seifert, A., Schlottke, J., and Weigand, B.: Numerical Investigation of Collision-Induced Breakup of Raindrops. Part II: Parameterizations of Coalescence Efficiencies and Fragment Size Distributions, Journal of the Atmospheric Sciences, 67, 576–588, https://doi.org/10.1175/2009JAS3175.1, 2010.

Sölch, I. and Kärcher, B.: A large-eddy model for cirrus clouds with explicit aerosol and ice microphysics and Lagrangian ice particle tracking, Quarterly Journal of the Royal Meteorological Society, 136, 2074–2093, https://doi.org/10.1002/qj.689, 2010.

Testik, F. Y. and Rahman, M. K.: First in situ observations of binary raindrop collisions, Geophysical Research Letters, 44, 1175–1181, https://doi.org/10.1002/2017GL072516, 2017.

Wood, R., Irons, S., and Jonas, P. R.: How Important Is the Spectral Ripening Effect in Stratiform Boundary Layer Clouds? Studies Using Simple Trajectory Analysis, Journal of the Atmospheric Sciences, 59, 2681–2693, https://doi.org/10.1175/1520-0469(2002)059<2681:HIITSR>2.0.CO;2, 2002.

Yin, Y., Levin, Z., Reisin, T. G., and Tzivion, S.: The effects of giant cloud condensation nuclei on the development of precipitation in convective clouds — a numerical study, Atmospheric Research, 53, 91–116, https://doi.org/10.1016/S0169-8095(99)00046-0, 2000.

Zhao, X. and Liu, X.: Primary and secondary ice production: interactions and their relative importance, Atmospheric Chemistry and Physics, 22, 2585–2600, https://doi.org/10.5194/acp-22-2585-2022, 2022.